Supporting Online Material

Materials and Methods

Construction of TPGA

The choice of the along-strike extent of the region used to calculate the local average trench-normal gravity profile is non-unique. Our choice corresponds to the regions outlined in Fig. S1. Each region incorporates at most the entire extent of a given subduction arc, and at a minimum, the rupture zone of several great earthquakes (Fig. 1B, Figs. S2, S3, S8). By construction, the TPGA in a given region will integrate to zero along any path a constant distance from the trench. In general, the gradients of TPGA discussed in this study are visible in the original free air gravity data (compare Figs. 1A and 1B). The removal of the average trench normal profile serves to put all subduction zones on a more comparable footing. The resulting TPGA primarily reflects short wavelength variations in shallow fore-arc structures (Fig. 1B), and can vary strongly in directions both parallel and perpendicular to the strike of the trench. There is no obvious systematic dependence of TPGA on the age of subducting plates or the type of overriding plate (continental or oceanic). We have used different sub-regions to calculate TPGA, and found very similar estimate of TPGA (Fig. S2).

Estimation of TPGA associated with subduction zone earthquakes

Because events in the relocated ISC and Harvard CMT catalogs are treated as point sources, we must assume a relationship between the size of the earthquake and the area that slipped. We assume a dip-slip rectangular fault with dimensions that scale with seismic moment and stress drop (*S1*). We consider extremal values of stress drops in the range of 1-10 MPa (*S2*). The slip area of each event is assumed to be square and centered on the hypocenter. If this assumption results in surpassing the surface or down dip limit of the slab interface, the assumed area becomes rectangular,

with the slipping area extending along strike. The CMT location is determined as the centroid of energy release and considered as the best available global dataset of seismic moment and location. The CMT catalogue we use spans the time period from 1976 to 2001, while the relocated ISC catalogue begins in 1900. For events in the ISC catalogue without a corresponding CMT-determined seismic moment, we estimate moment via a moment-magnitude relationship (*S3, S4*).

The distribution of co-seismic slip for the three largest earthquakes may be complicated and our assumed hypocenter, fault area, and computed mean TPGA, may thus not adequately approximate reality. Therefore, for these three events, we use available distributed slip models (*S5, S6, S7*) to compute their associated TPGA.

Construction of TPTA

As with the TPGA, we bin the TPTA in four groups with equal total area in a given range of TPTA. We note that ETOPO-5 data is not as highly resolved as the gravity data (*S8, S9*). Gravity data is higher solution with 30 sec grid spacing while ETOPO-5 data is with 5 min grid spacing. Track lines used to construct ETOPO-5 are denser in along the convergent plate boundary (refer Fig. 1 in S9,) the error due to griding is not likely to be significant at the scales we are interested (several tens of kilometers).

Supporting Online Text

Moment release vs. TPGA

We first consider the distribution of moment for individual events versus TPGA (Fig. S3). For events in either the CMT or the ISC catalogues, no great earthquakes (Mw≥8.0) occur in areas with positive TPGA (> 40 mGal). Given the large number of events involved, we find it useful to also consider the distribution of cumulative moment (Fig. S4). We observe that about 80% of the cumulative moment is produced in 30% of total area of subduction zone with TPGA less than -30 mGal, while less than 20% of cumulative moment is produced in the 70% of the area of subduction zone with TPGA greater than −30 mGal. The total cumulative seismic moment is dominated by the three largest earthquakes of the 20^{th} century. When excluding the three largest earthquakes, we find that about 45% of the remaining total seismic moment is produced in about 25% of the total area of subduction zone with highly negative TPGA (< -40 mGal).

Robustness of correlation between TPGA and seismic moment

Despite the inherent limitations of the global earthquake catalogues, such as event mislocation and incompleteness, the correlation between TPGA and the occurrences of large earthquakes does not depend on the assumed magnitude of the stress drop, which catalog is used, or how seismic moment is distributed over a given earthquake's fault area (Fig. S5 and Fig. S6). In addition, Monte-Carlo permutation tests (*S10*) indicate that the difference in total seismic moment between areas with strongly negative TPGA (< −40 mGal) and areas with strongly positive TPGA (> 40 mGal) is significant at a 95% confidence level.

Supporting Online Figure S1

Caption Figure S1: Location of the subduction zones considered in this study: **(A)** Alaska-Aleutian **(B)** Kamchatka-Kurile **(C)** Japan **(D)** Nankai **(E)** Ryukyu **(F)** Izubonin-Mariana **(G)** Sumatra-Java **(H)** Tonga-Kermadec **(I)** Chile **(J)**, northern South America, **(K)** Central America and **(L)** Cascadia. Average trench-normal profiles are computed using the regions as outlined.

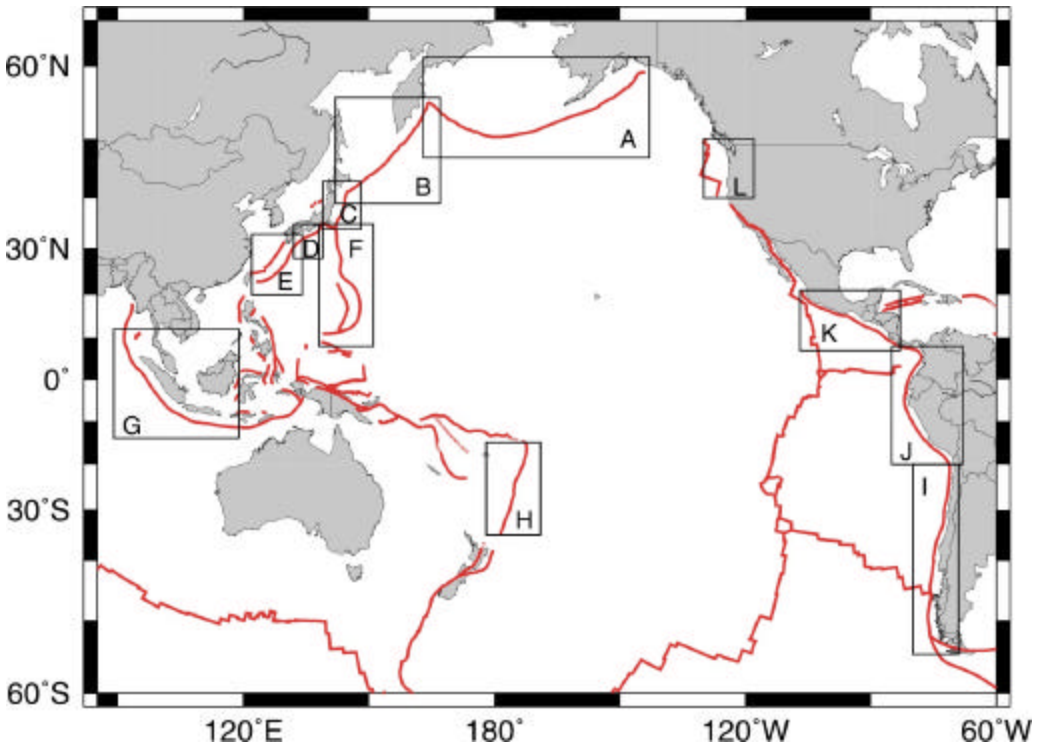

Supporting Online Figure S2

Caption Figure S2: TPGA computed using different sub-regions for **(A)** Alaska **(B)** Aleutian **(C)** Kamchatka **(D)** Kurile, respectively. The average trench-normal gravity profile is calculated for the region shown in the inset and shown in the sub-panel of Fig. 1A. The x-axis is trench-normal distance in degrees and the y-axis is gravity in mGal. The color bar shows the amplitude of the free-air gravity anomaly. subduction zone earthquakes from the ISC (1900-1976) with M_w=7.5 and Harvard CMT (1976-2001) catalogues with M_w=7.0, are plotted as solid circles and moment tensors, respectively. Trench location (*S11*) and 50-km slab iso-depth contour (*S12*) are indicated by the barbed and thick black lines, respectively. Directions of relative plate convergence (*S13*) are shown as arrows.

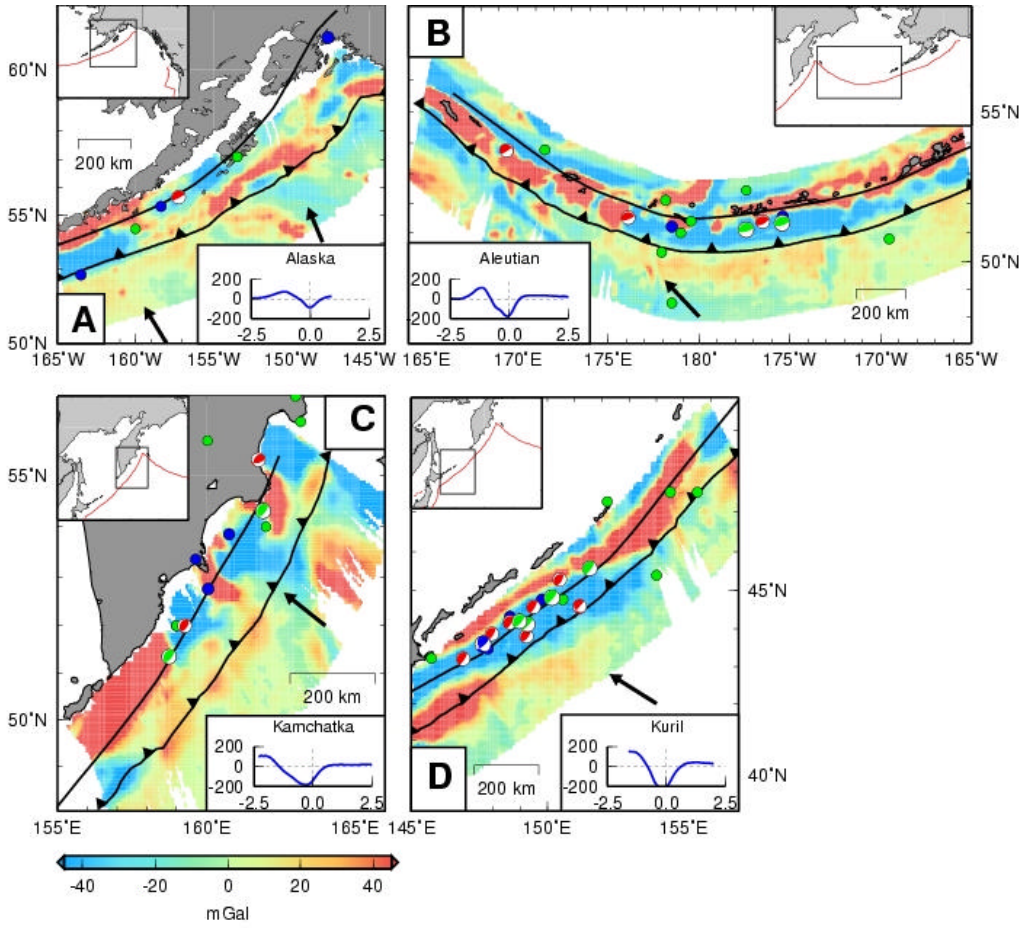

Supporting Online Figure S3

Caption Figure S3: **(A)** Observed TPGA in the Southern Chile subduction zone. Average trench-normal profile is computed in region (I) shown in Fig. S1. Black solid line represents 10 m contour of co-seismic slip of the 1960 Chilean earthquake (*S14*). **(B)** Observed TPGA in Kamchatka-Kurile. Previously documented seismic gap (*S15*) is shown by a black bar. Areas with large moment released during 1952 great earthquakes are indicated in black boxes (*S16*). Symbol descriptions follow Fig. S2.

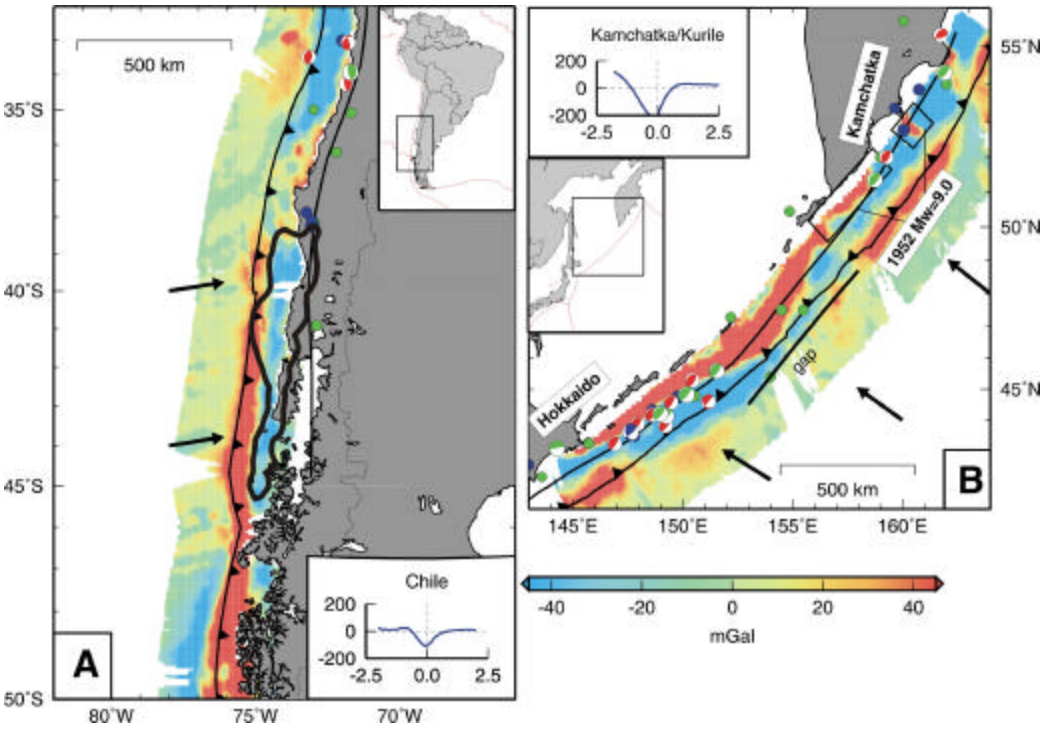

Supporting Online Figure S4

Caption Figure S4: Scatter plot of M_w vs. TPGA. Solid and open circles indicate data from CMT and ISC catalogue, respectively. Cumulative percent of total seismic moment with respect to TPGA for the entire ISC catalogue, ISC catalogue with M_w<9.0, and CMT catalogue are shown with green, red and blue lines, respectively. Mean TPGA for the three giant events are calculated using available slip models (*S14, S16, S17*). Dashed lines indicate the values of TPGA that divide the total area of subduction zone interface into four bins of approximately equal area.

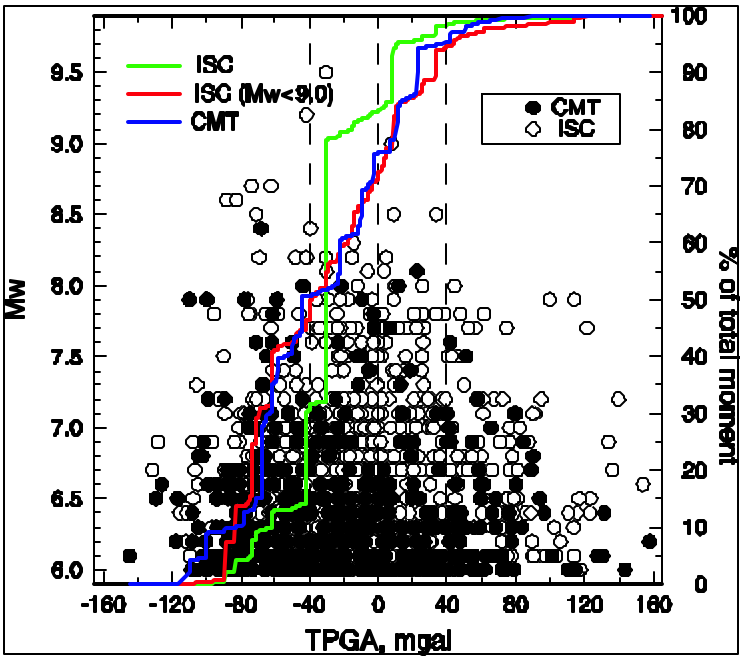

Supporting Online Figure S5

Caption Figure S5: Histogram of total seismic moment vs. TPGA for **(A)** All CMT events (1976-2001) with M_w=6.0. **(B)** All events with M_w=6.0 located in both CMT and ISC catalogues (1976-2001). A 10 MPa stress drop is assumed when estimating slip area. **(C)** All ISC events in 1900-1976. **(D)** All CMT events (1976-2001) and ISC events (1900-1976).

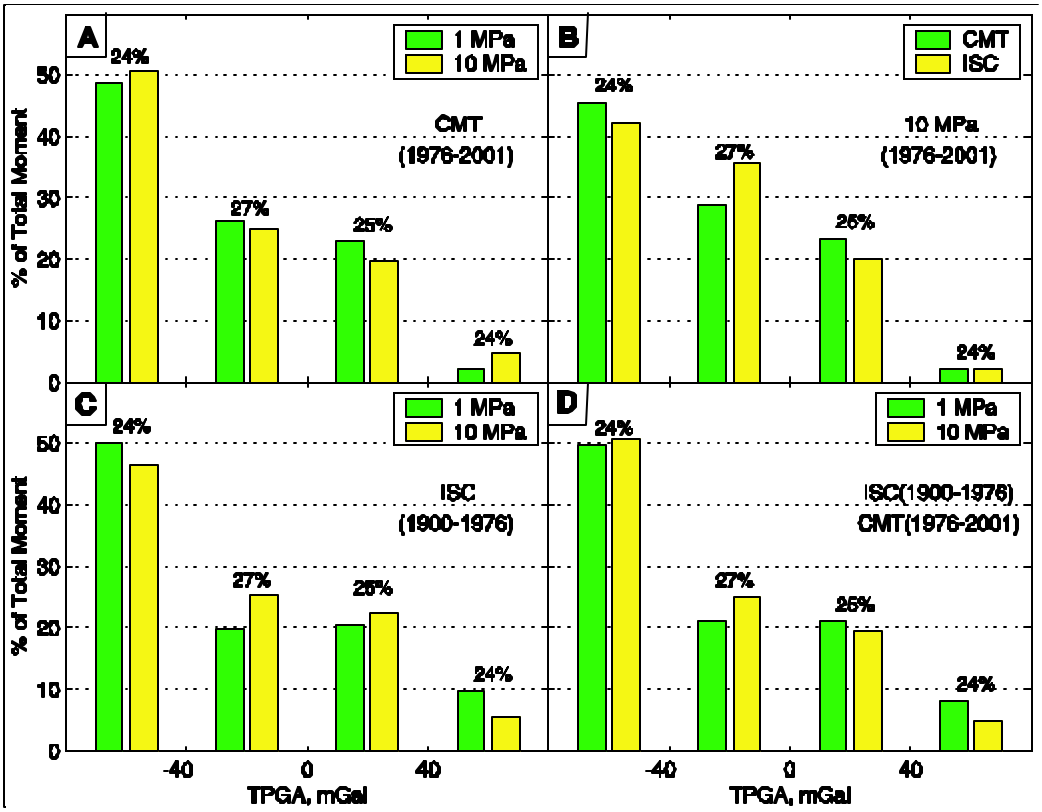

Supporting Online Figure S6

Caption Figure. S6: Histogram of total seismic moment vs. TPGA derived using an alternative approach from that used in all other figures. Here we do not calculate the average TPGA for a given earthquake. Instead, the plate interface is pixilated into small (about 0.1 x 0.1 deg) cells of constant TPGA, and the seismic moment for a given earthquake is evenly distributed onto the cells within the estimated fault area. We then form the histogram by evaluating the total distributed moment in cells lying within a given range of TPGA. **(A)** All CMT events (1976-2001) with M_w=6.0. **(B)** All ISC events from 1900-1976. The percent of the slab interface area represented by each bin is shown above each bar.

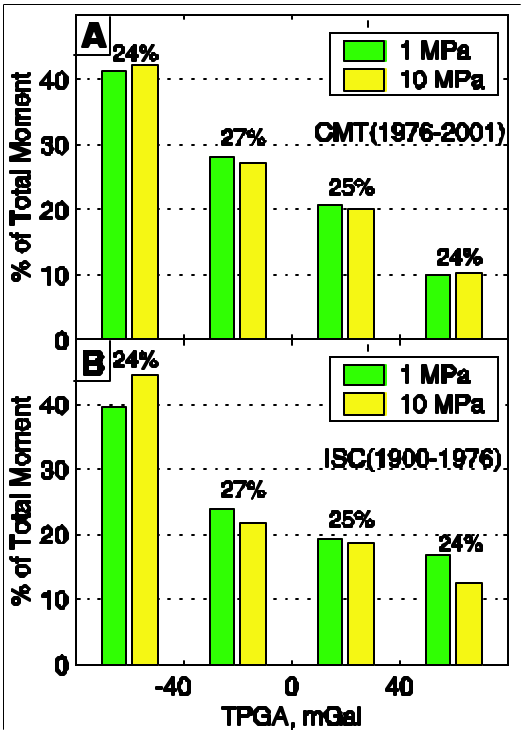

Supporting O nline Figure S7

Caption Figure S7: Seismic moment release vs. TPGA and TPTA using all CMT events with M_w=6.0 assuming a 1 MPa stress drop to calculate the slip area. **(A)** Number of event **(B)** percent of slab interface area **(C)** percent of seismic moment **(D)** Seismic moment density.

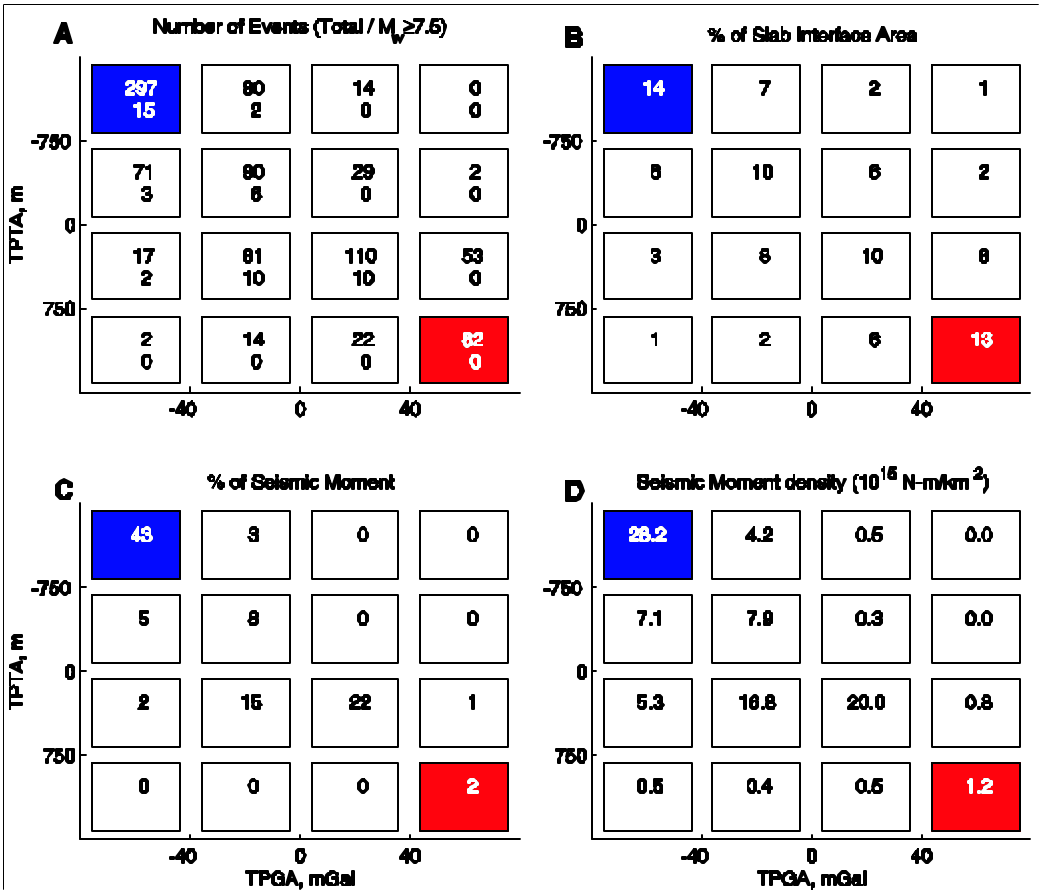

Supporting Online Figure S8

Caption Figure S8: **(A)** Observed TPGA in Kermadec. The average trench-normal profile is computed in region H shown in Fig. S1. Contours indicate sediment thickness (*S18*) in meters. **(B)** Observed TPGA in northern S. America. The extent of previously determined seismic gap (*S15*) is shown with a black bar. Symbol descriptions follow Fig. S2.

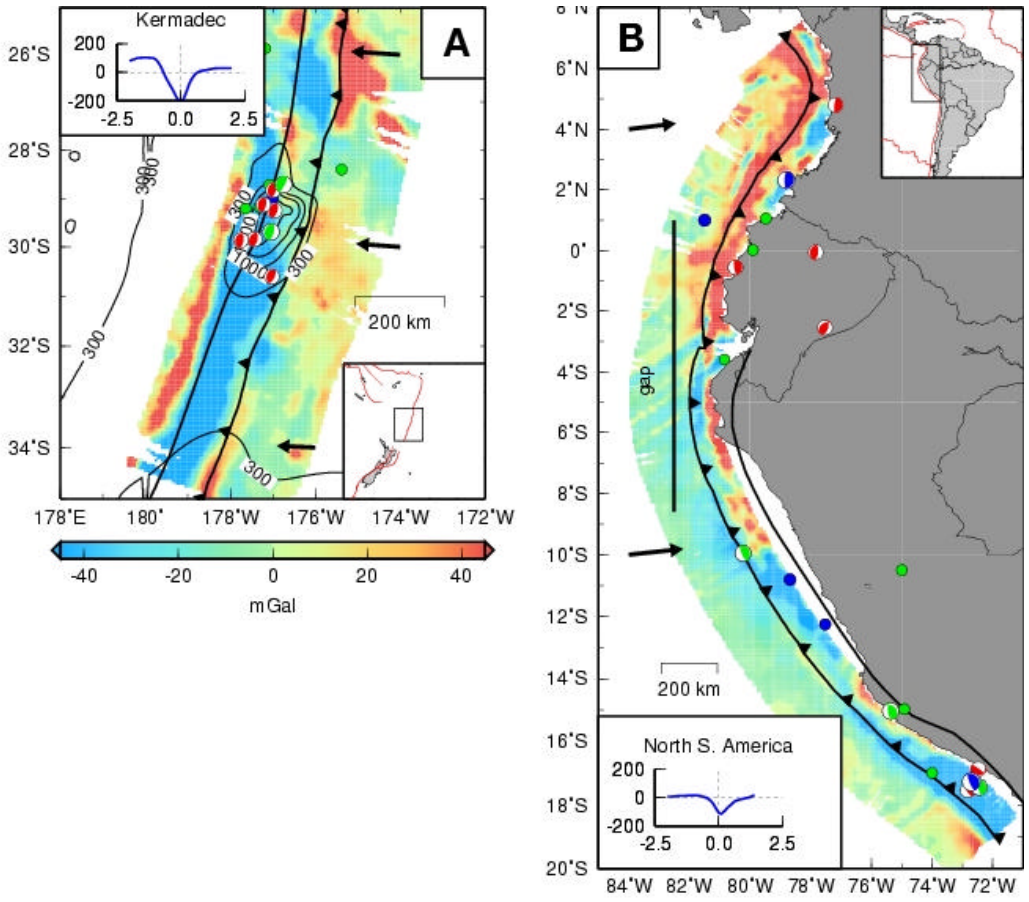

References for Supporting OnlineMaterial

S1. T. Lay, T. Wallace, in *Modern Global Seismology,* 521p (1995).

S2. H. Kanamori, D. L. Anderson, *Bull. Seis. Soc. Am.* **65**, 1073-1095 (1975).

S3. P. Chen, H. Chen, *Tectonophysics* **166**, 53-72 (1989).

S4. H. Kanamori, *Tectonophysics* **93**, 185-199 (1983).

S5. L. Ruff, H. Kanamori, *Phys. Earth Planet. Inter.* **31**, 202 (1983).

S6. S. E. Barrientos, S. N. Ward, *Geophys. J. Int.* **103**, 589 (1990).

S7. J. M. Johnson, K. Satake, *Pure Apply. Geophysics.* **154**, 541 (1999).

S8. National Geophysical Data Center, ETOPO-5 bathymetry/topography data, *Data Announc.* 88-MCG-02, Natl. Oceanic and Atmos. Admin. U. S Dep. Commer., Boulder, Colo. (1988).

S9. W. H. F. Smith, *J. Geophys. Res.* **98**, 9591 (1993).

S10. E. L. Lehmann, in *Testing Statistical Hypothesis.* Wiley publication in statistics, 369 pp (1959).

S11. National Geophysical Data Center, Global Relief data (CD-ROM). World data center for marine geology and geophysics, Boulder, Colo. (1993)

S12. O. Gudmundsson, M. Sambridge, *J. Geophys. Res*. **103**, 7121 (1998).

S13. C. DeMets, R. G. Gordon, D. F. Argus, *Geophys. Res. Lett.* **21**, 2191 (1994).

S14. S. E. Barrientos, S. N. Ward, *Geophys. J. Int.* **103**, 589 (1990).

S15. T. Lay, H. Kanamori, L. Ruff, *Earthquake Pred. Res.* **1**, 1 (1982).

S16. J. M. Johnson, K. Satake, *Pure Apply. Geophysics.* **154**, 541 (1999).

S17. L. Ruff, H. Kanamori, *Phys. Earth Planet. Inter.* **31**, 202 (1983).

S18.National Geophysical Data Center, Total Sediment Thickness of the World's Oceans & Marginal Seas, Natl. Oceanic and Atmos. Admin. U. S Dep. Commer., Boulder, Colo. (1996).